SCIENTIFIC PAPERS
OF THE UNIVERSITY OF PARDUBICE
Series A
Faculty of Chemical Technology
4 (1998)

PREPARATION AND CHARACTERIZATION OF $(Bi_{1-x}Sb_x)_2Se_3$ SINGLE CRYSTALS

Čestmír DRAŠAR[a1] and Petr LOŠŤÁK[b]
[a]Department of Physics,
[b]Department of General and Inorganic Chemistry,
University of Pardubice, CZ-532 10 Pardubice

Received April 6, 1998

This review paper summarizes papers dealing with characterization of $(Bi_{1-x}Sb_x)_2Se_3$ single crystals which have been produced at the Faculty of Chemical Technology, University of Pardubice. The single crystals of $(Bi_{1-x}Sb_x)_2Se_3$, prepared by a modified Bridgman method, were characterized by means of the X-ray diffraction analysis, homogeneity assessment, and by measurements of the reflectance in the plasma resonance range, transmittance, electric conductivity $\sigma \perp c$, Hall constant $R_H(\mathbf{B} \parallel c)$, Seebeck coefficient $\alpha(\Delta T \perp c)$ and by figure of merit Z. The model of point defects in single crystals $(Bi_{1-x}Sb_x)_2Se_3$ is used for qualitative explanation of the changes in physical properties induced by incorporation of Sb atoms into Bi_2Se_3.

[1] To whom correspondence should be addressed.

Introduction

During the past tens of years semiconductors stimulated rapid industrial development. Semiconductors are necessary for telecommunication, computers, industry, and so on. The last decade or so increased attention has been paid to thermoelectric materials when operated in both the Peltier mode (refrigeration) and in the Seebeck mode (generation of electricity). Both the thermoelectric generators and the thermoelectric coolers are widely employed in science, industry, etc.

An electrical voltage (absolute Seebeck voltage, ASV) is generated within any conducting material (metal, semiconductor) that is subjected to a temperature gradient. This phenomenon is referred to as absolute *Seebeck effect*. The absolute Seebeck coefficient, ASC = $[d(ASV)/dT]_T$. The thermocouple is made of two dissimilar conductors A and B by electrically joining one set of their ends. A temperature difference between the joined set and unjoined set of ends of the thermocouple produces a voltage (relative Seebeck voltage, RSV) between the unjoined ends. The relative Seebeck coefficient, RSC = $[d(\mathrm{RSV})/dT]_T$ = $\mathrm{ASV_A} - \mathrm{ASV_B}$. This enables to determine the ASC of any material. This device can produce electricity.

When current flows across the junction of conductors A and B, a reversible heat is liberated or consumed at the junction. This phenomenon is referred to as *Peltier effect*. The amount of heat is proportional to the current and RSC. This effect is mostly employed for construction of thermoelectric coolers as illustrated below.

Exploitation of thermoelectric generators:

- cathodic protection of gas and oil pipelines and well casing
- telecommunications in sites where electricity is not accessible
- space devices

Exploitation of thermoelectric coolers:

- cooling high power electronic element
- construction of thermostats and coolers in laboratories
- medicinal use as cryoscalpels, coolers for blood, insulin, etc.

The so-called figure of merit $Z = \sigma\alpha^2/\kappa$ (where σ is electrical conductivity, α Seebeck coefficient and κ thermal conductivity) is employed in the rearch of potentially good thermoelectric materials. It is evident that the higher electrical conductivity, the higher Seebeck coefficient, and the lower thermal conductivity the material possesses the better is its efficiency when working as both the coolers and the generators. Regarding the above-mentioned facts, the best materials for thermoelectric applications are semiconductors. They possess available and easily controlled electrical conductivity and Seebeck coefficient and moderate thermal

conductivity. Moreover, the formation of single phase solid solution of the compounds with the identical cation or anion leads to a decrease in magnitude of lattice thermal conductivity. Regarding this fact, especially the solid solutions are used in thermoelectric applications and often studied.

Solid solutions on the basis of narrow-gap semiconductors $A_2^{V}B_3^{VI}$ (where A = Bi, Sb and B = Se, Te) of tetradymite structure (space group D_{3d}^5) fall into the group of materials used in thermoelectric applications [1]. Therefore materials of this type are the object of both theoretical and applied research.

Regarding the possible usage in above mentioned applications our attention was focused on the solid solutions of Bi_2Se_3 - Sb_2Se_3, i.e. mixed crystals $(Bi_{1-x}Sb_x)_2Se_3$.

Despite considerable attention given to the research of Bi_2Se_3 (Refs. [2–4]), there are very few data in the literature on the physical properties of the mixed crystals in the Bi_2Se_3 - Sb_2Se_3 system. It follows from the phase diagram presented by Kuznetsov et al. [5] that some substitutional solid solutions on the basis of Bi_2Se_3 tetradymite exist in this system. From DTA and X-ray analysis it was found that the phase diagram of Bi_2Se_3 - Sb_2Se_3 system is described by a peritectic diagram (the peritectic temperature 640 ± 3 °C). X-ray analysis revealed that substitutional solid solutions of tetradymite structure in the concentration interval from 0 to 16.2 mol.% Sb_2Se_3 and orthorhombic structure in the concentration interval from 52.5 to 100 mol.% Sb_2Se_3 exist up to 500 °C.

The electrical conductivity and Seebeck coefficient were measured on the polycrystalline samples [6]. The electrical conductivity decreased from 2.7×10^{-3} $\Omega^{-1}\,cm^{-1}$ to 8.3×10^{-7} $\Omega^{-1}\,cm^{-1}$ and the Seebeck coefficient increased from 70 $\mu V\,K^{-1}$ to more than 700 $\mu V\,K^{-1}$.

A characterization of single crystal of solid solution $(Bi_{0.3}Sb_{0.7})_2Se_3$ of rhomboedric structure is given in paper [7]. Transmittance, photoeffect, Hall constant, and electrical conductivity were measured.

It is evident that information about physical properties of $(Bi_{1-x}Sb_x)_2Se_3$ single crystals are not available in the literature. This review paper summarizes results of research into this system carried out at the University of Pardubice.

Preparation and Basic Characterization of $(Bi_{1-x}Sb_x)_2Se_3$ Single Crystals

Preparation of single crystals of $(Bi_{1-x}Sb_x)_2Se_3$ composition and X-ray diffraction analysis were described in an earlier paper [8]. A great deal of attention was given to investigation of homogeneity of the crystals.

$(Bi_{1-x}Sb_x)_2Se_3$ single crystals were grown using a modified Bridgman method. The starting polycrystalline materials were synthesized from the semiconductor purity (5 N) elements in conical silica ampoules evacuated to a residual pressure of 10^{-4} Pa in a horizontal furnace at a temperature of 1073 K for 48 hours. The ampoule charged with the polycrystalline material was then suspended into the upper hot zone of a Bridgman furnace (see the scheme in Fig. 1) where it was heated at a temperature of 1073 K for 24 hours. During the heat treatment the ampoule was several times violently agitated in order to allow the melt to fill perfectly the conical tip, which is an important prerequisite of the growth of perfect crystals. Then the ampoule was lowered into the temperature gradient, the profile of which is shown in Fig. 1, at a rate of 1.3 mm hour^{-1}.

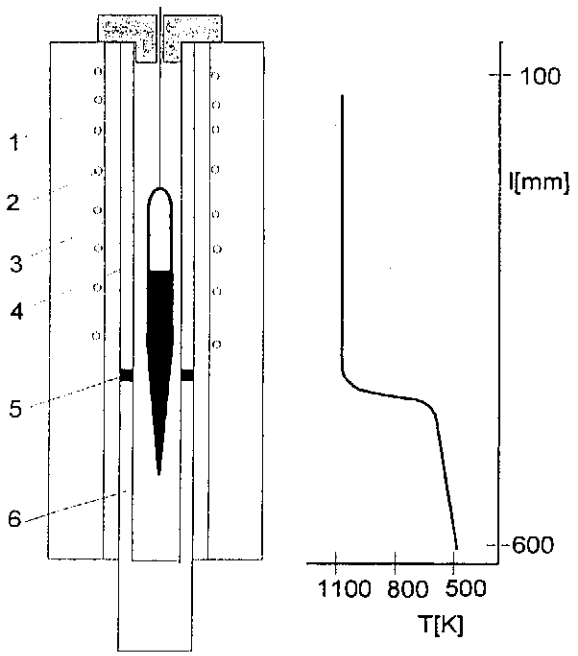

Fig. 1 Schematic drawing of the furnace for the growth of $(Bi_{1-x}Sb_x)_2Se_3$ crystals and the temperature gradient used: 1 – thermal insulation (asbestos), 2 – resistance heating, 3 – ceramic tube, 4 – stainless-steel tube, 5 – asbestos ring, 6 – copper tube, 7 – cooling

The procedure described enabled us to grow well cleavable single crystals approximately 50 to 60 mm long, 10 mm in diameter; their trigonal axis *c* was in all cases parallel to the axis of ampoule. The orientation of the cleavage faces was checked using the Laue back diffraction technique.

The antimony content in the samples was determined using an energy dispersive X-ray analyzer Kevex Delta 5 with Quantum detector. The conditions are described in the paper [8].

With the aim to investigate the homogeneity of the crystals, in addition to quantitative analysis, the distribution of antimony and bismuth across the cleavage faces were analyzed in the directions parallel and perpendicular to the crystal axis.

Lattice Parameters of $(Bi_{1-x}Sb_x)_2Se_3$ Crystals

The lattice parameters of the single crystal samples prepared were determined on powder samples by X-ray diffraction analysis using an HZG-4B diffractometer (Freiberger Präzisionsmechanik, Germany). The diffraction maxima were measured by means of a step procedure at a step of 0.01° with CuK_α radiation; the K_β radiation was removed using a nickel filter. The calibration of the diffractometer was carried out with polycrystalline silicon. The diffraction lines obtained were indexed according to Gobrecht et al. [9] and the values of the lattice parameters a and c of the crystals were calculated by the least squares method.

Tab. I Lattice parameters of $(Bi_{1-x}Sb_x)_2Se_3$ crystals

x	a nm	c nm	V nm^3	c/a	$\Delta 2\vartheta$ *)
0	0.41386(4)	2.8620(2)	0.4245	6.915	0.005
0.005	0.41384(3)	2.8629(2)	0.4256	6.918	0.0056
0.023	0.41337(6)	2.8619(4)	0.4236	6.922	0.0098
0.071	0.41285(5)	2.8636(4)	0.4227	6.936	0.0093
0.081	0.41279(3)	2.8636(2)	0.4226	6.937	0.0056
0.135	0.41220(6)	2.8636(4)	0.4214	6.947	0.0106
0.276	0.41172(9)	2.8644(6)	0.4205	6.957	0.015

*) $\Delta 2\vartheta = \sum_{1}^{N} \left| 2\vartheta_{exp} - 2\vartheta_{calc} \right| / N$, where $2\vartheta_{exp}$ is the experimental diffraction angle, $2\vartheta_{calc}$ is the angle calculated from lattice parameters and N is number of investigated diffraction lines.

The results of the X-ray diffraction analysis of $(Bi_{1-x}Sb_x)_2Se_3$ crystals are given in Table I. It is evident that the incorporation of Sb atoms into the Bi_2Se_3 crystal lattice results in a decrease of the a parameter, increase of the c parameter and of the c/a ratio, and a decrease of the unit cell volume V of the crystal lattice. These changes are in good agreement with the results reported by Kuznetsov et al.

[5], according to which in the range of the solid solutions of tetradymite structure in the Bi_2Se_3 – Sb_2Se_3 system the value of the a parameter decreases from 0.4140 nm to 0.4118 nm while the c/a ratio increases. If we compare the values of the atomic radii of bismuth and antimony (r_{Bi} = 0.151 nm, r_{Sb} = 0.144 nm), we can adopt the conclusion that the observed decrease in the volume V testifies the formation of a substitutional solid solution, i.e. the formation of mixed $(Bi_{1-x}Sb_x)_2Se_3$ crystals. In the first approximation, actually, it is plausible to assume that the substitution of smaller antimony atoms for Bi atoms in the Bi_2Se_3

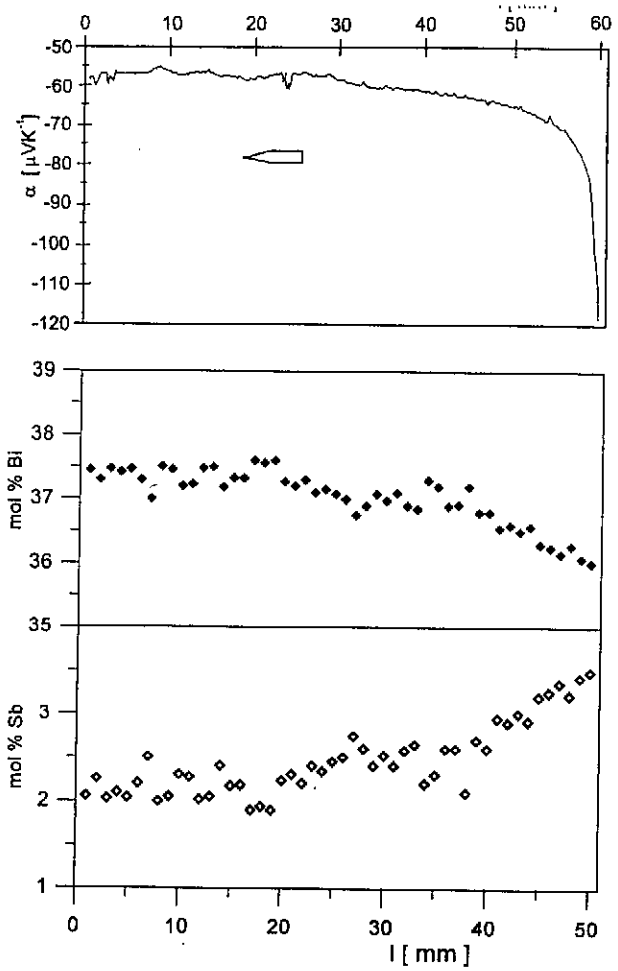

Fig. 2 Comparison of the variations of the Seebeck coefficient measured on the cleavage face of a $Bi_{1.89}Sb_{0.11}Se_3$ crystal in the direction of the crystal axis with the results of the determination of bismuth and antimony content

crystal lattice gives rise to a decrease of the unit cell volume.

The diffractograms of all samples showed only the lines corresponding to the tetradymite structure; the prepared $(Bi_{1-x}Sb_x)_2Se_3$ crystals are thus classified under the $D_{3d}^5 = R\bar{3}m$ space group symmetry. This fact is also in accordance with Kuznetsov et al. [5], according to whom a region of solid solutions with tetradymite structure exists in the Bi_2Se_3 - Sb_2Se_3 system.

Homogeneity of $(Bi_{1-x}Sb_x)_2Se_3$ Crystals

In view of the selected method of preparation of $(Bi_{1-x}Sb_x)_2Se_3$ single crystals from the melt, great attention was paid to assessment of the homogeneity of the crystals grown. On the basis of comparing the melting points of both components of the Bi_2Se_3 - Sb_2Se_3 system (according to Abrikosov et al. [10] the melting point of Bi_2Se_3 equals 706 °C, according to Wobst [11] the melting point of Sb_2Se_3 equals 590 °C) one can expect a non-negligible gradient in the antimony content along the crystal axis, from the tip to the upper end. In fact, it can be assumed that on growing the mixed crystals by the Bridgman method the tip of the crystal will contain excess concentration of the component with higher melting point, i.e. Bi_2Se_3; towards the upper part of the crystal one can thus expect a gradual increase in the concentration of the component with lower melting point—i.e. Sb_2Se_3.

Assuming that the incorporation of Sb atoms into the Bi_2Se_3 crystal lattice results in a change of the free carrier concentration N, the expected gradient will have to affect the values of all the quantities depending on N. For this reason the homogeneity was tested by measuring the variations of the Seebeck coefficient, using the probe described in paper [12]. The results obtained are shown in Fig. 2 for a crystal of composition $(Bi_{0.945}Sb_{0.055})_2Se_3$; the variation of the Seebeck coefficient α along the crystal axis is confronted here with the results of the determination of the Sb and Bi content by means of the energy dispersive analyzer. It is evident from the $\alpha = f(l)$ dependence that from the tip up to the distance of about 15 mm from the upper end of the crystal the Seebeck coefficient is nearly constant. Closer to the upper end, there is a marked increase in the α value. The analysis of the Sb and Bi content is in good agreement with this observation: the concentration of both analyzed elements remains virtually unchanged in that part of the crystal where the Seebeck coefficient was nearly constant, whereas there is a clear increase of the Sb content and a decrease of the Bi content in the upper part of the crystal.

The homogeneity was investigated not only along the axis of the crystals but also in the direction perpendicular to the pulling direction, across the crystal. Fig 3. shows the variations of the Seebeck coefficient on the cleavage face in the direction perpendicular to the crystal axis, at a distance of 10 mm from the upper end of the $(Bi_{0.945}Sb_{0.055})_2Se_3$ crystal. From this figure it is clear that in the central part of the crystal the value of the Seebeck coefficient is practically constant, whereas near the

edges (at the surface) of the crystal the α values abruptly increase. It follows from the results of the analysis of Bi and Sb content that the observed $\alpha = f(l)$ dependence in this direction does not correlate with the concentration gradient of antimony or bismuth. Besides, in this direction—perpendicular to the pulling direction—no Bi or Sb concentration gradient is expected. To this result we add that analogous $\alpha = f(l)$ dependences in the direction perpendicular to the pulling direction were observed in $Bi_{2-x}In_xSe_3$ crystals, whose preparation and properties

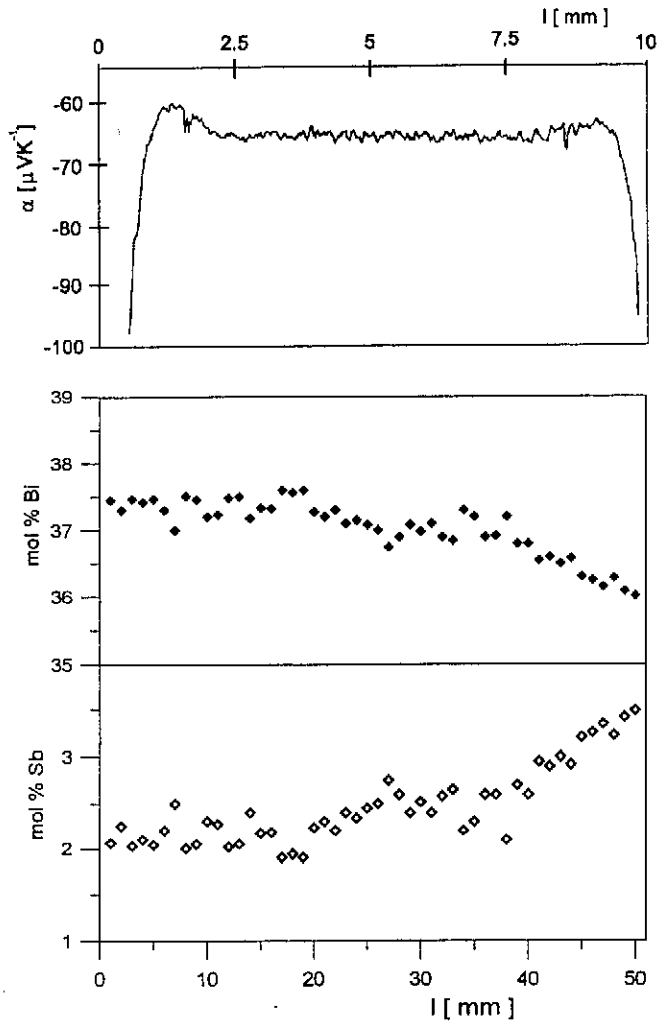

Fig. 3 Comparison of the variations of the Seebeck coefficient measured on the cleavage face of a $Bi_{1.89}Sb_{0.11}Se_3$ crystal in the direction perpendicular to the crystal axis with the results of the determination of bismuth and antimony content

have been presented in one of our earlier communications [13]. The observed rise of the α values near the crystal surface can be—in our opinion—explained in much the same way as in paper [13].

It is well known that on growing Bi_2Se_3 from the melt of stoichiometric composition the obtained crystals show always superstoichiometric bismuth content [14]; selenium partially segregates on the crystal surface. On passage of the crystal through the temperature gradient in the Bridgman furnace at temperatures close to the melting point one cannot exclude the possibility of diffusion of selenium, segregated at the surface, into the crystal. Taking into account the idea that selenium substoichiometry in the Bi_2Se_3 crystal lattice results in dominant formation of positively charged selenium vacancies $V_{Se}^{\bullet}$ or $V_{Se}^{\bullet\bullet}$ whose charge is compensated by free electrons [15,16], the diffusion of selenium into the surface layers of the crystal, where it occupies selenium vacancies, seems to be acceptable. Occupation of $V_{Se}^{\bullet}$ and/or $V_{Se}^{\bullet\bullet}$ vacancies then leads to a suppression of the free electron concentration. This, in turn, is manifested by the increase of the Seebeck coefficient near the crystal surface. Owing to the fact that the charge for the crystals prepared was weighed in the stoichiometry corresponding to the formula $(Bi_{1-x}Sb_x)_2Se_3$, the segregation of selenium has to be taken into account. That is why this idea is well acceptable.

The suppression of the concentration of free electrons in Bi_2Se_3 by annealing the crystals in selenium atmosphere, leading to a decrease of the electric conductivity and to an increase in the Hall constant and Seebeck coefficient values, as presented by e.g. Gobrecht et al. [17], supports the above-discussed explanation of the experimentally determined dependence $\alpha = f(l)$ in the direction perpendicular to the pulling axis of the crystal.

Hence we can state that, under given conditions of preparation, the $(Bi_{1-x}Sb_x)_2Se_3$ mixed crystals were essentially homogeneous, except for the 15 mm wide region at their upper end.

Optical Properties of $(Bi_{1-x}Sb_x)_2Se_3$ Crystals

Single crystals of $(Bi_{1-x}Sb_x)_2Se_3$ prepared by the Bridgman technique [8] were characterized by the measurements of transmittance in the IR region and reflectance in plasma resonance region. The results are summarized in paper [18].

Spectral dependences of the reflectance R were measured at room temperature in unpolarized light on natural (0001) cleavage faces using a FT-IR spectrometer Biorad FTS 45. The geometry of the experiment was such that the electric field vector $\boldsymbol{E}$ of the electromagnetic radiation was always perpendicular to the trigonal c-axis, i.e. $\boldsymbol{E} \perp c$.

The measurements of the transmittance spectra on thin samples were carried out at room temperature using the same spectrometer. The radiation was unpolarized, but the orientation of the samples with respect to the incident radiation

always fulfilled the condition $\boldsymbol{E} \perp c$.

Reflectance

It is evident from Fig. 4, where the reflectance spectra of the $(Bi_{1-x}Sb_x)_2Se_3$ samples are shown, that the reflectance in the plasma resonance frequency range exhibits a pronounced minimum. The locations of the corresponding reflectance minima ν_{min} of individual samples are given in Table II. These data together with Fig. 4 imply that the incorporation of Sb atoms into the Bi_2Se_3 crystal lattice in the range of low Sb concentrations gives rise to a shift of the reflectance minima towards higher wavenumbers (sample No. 2). The reflectance minima of the samples with higher Sb content are, on the contrary, situated at lower wavenumbers, as compared to the location of the minimum for nominally "pure" Bi_2Se_3.

Experimental $R(\nu)$ dependences were modelled using the relations for the real (ε_1) and imaginary (ε_2) parts of the complex dielectric function, following the Drude–Zener theory [19]

$$\varepsilon_1 = n^2 - k^2 = \varepsilon_\infty \left(1 - \frac{1}{\left(\frac{\omega}{\omega_p}\right)^2 + \left(\frac{1}{\omega_p \tau}\right)^2} \right) \tag{1}$$

$$\varepsilon_2 = 2nk = \frac{\varepsilon_\infty}{\omega\tau} \frac{1}{\left(\frac{\omega}{\omega_p}\right)^2 + \left(\frac{1}{\omega_p \tau}\right)^2} \tag{2}$$

where n is the index of refraction, k is the index of extinction, τ is the optical relaxation time, ε_∞ is the high-frequency permittivity, and ω_p is the plasma resonance frequency. For one type of carriers, the last quantity is given by the relation

$$\omega_p = \left(\frac{Ne^2}{\varepsilon_0 \varepsilon_\infty m_\perp} \right)^{1/2} \tag{3}$$

where $m_\perp$ is the free carrier effective mass in the direction perpendicular to the trigonal axis c, N is the concentration of free carriers, and ε_0 is the permittivity of

the free space. Approximate trial values of ε_∞, τ and ω_p were introduced in equations (1) and (2), and a suitable computer program was used to minimize the function $\sum_{n=1}^{m} (R_n' - R_n)^2$, where R' is the experimental reflectance, and R is the calculated value given by the relation

$$R = \frac{(n-1)^2 + k^2}{(n+1)^2 + k^2} \quad . \tag{4}$$

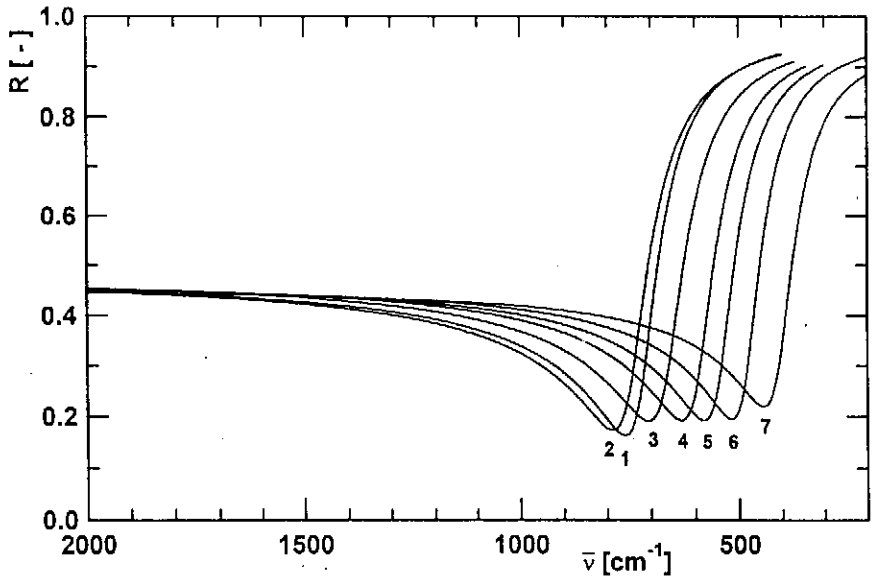

Fig. 4 Reflectance spectra of $(Bi_{1-x}Sb_x)_2Se_3$ samples (the samples are labeled according to Table II)

Using the fitted values of ε_∞ and ω_p, we determined from relation (3), the values of the ratio $N/m_\perp$ which yield data on the concentration of the free charge carriers, in our case free electrons. The results of this analysis are summarized in Table II.

It is evident from this table that low concentrations of Sb built into the lattice of Bi_2Se_3 result in an increase in the values of the plasma resonance frequency as well as in the ratio $N/m_\perp$; both these values decrease in the range of higher Sb content. Taking, in the first approximation, the free carrier effective mass $m_\perp$ to be constant, it is obvious that the substitution of Sb for Bi atoms in the crystal lattice of Bi_2Se_3 gives rise to an increase of the free carrier concentration in the range of low Sb concentration, whereas in the range of higher Sb content the free carrier

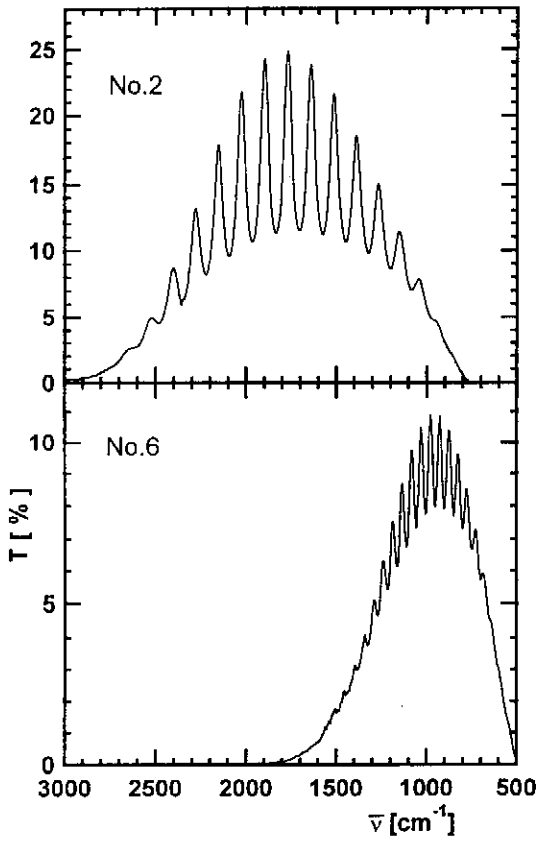

Fig. 5 Transmittance spectra of $(Bi_{1-x}Sb_x)_2Se_3$ crystals: Sample 2 – x = 0.012 (d = 7.9 μm); Sample 3 – x = 0.136 (d = 20.3 μm)

concentration is suppressed. This conclusion is in accordance with the results of the measurements of the Hall constant, electric conductivity and Seebeck coefficient, which we used in Ref. [8] to characterize the $(Bi_{1-x}Sb_x)_2Se_3$ crystals.

The values of the other quantities, i.e. the optical relaxation time τ and the high-frequency permittivity ε_∞, obtained from the interpretation of the reflectance spectra, do not show any appreciable variation with increasing value of x in the $(Bi_{1-x}Sb_x)_2Se_3$ samples. It is only worthwhile to note that ε_∞ tends to decrease slightly in the samples with the highest Sb content (samples Nos 6 and 7), which indicates that the substitution of Sb atoms for Bi in the Bi_2Se_3 lattice brings about an increase in the ionicity of the crystals studied.

Transmittance

As an illustration of the transmittance measurements, the $T = f(\nu)$ plots are presented for samples Nos 2 and 6 in Fig. 5. Well-developed interferences and a relatively high overall transmittance indicate a good optical quality of the crystals prepared.

The transmittance T and reflectance R values corresponding to the locations of the interference maxima in the $T = f(\nu)$ plot were used in the formula

$$K = \frac{1}{d}\ln\left\{\frac{1}{T}\left[\frac{1}{2}(1 - R^2) + RT + \frac{1}{2}\sqrt{(1 - R)^4 + 4RT(1 - R)^2}\right]\right\} \qquad (5)$$

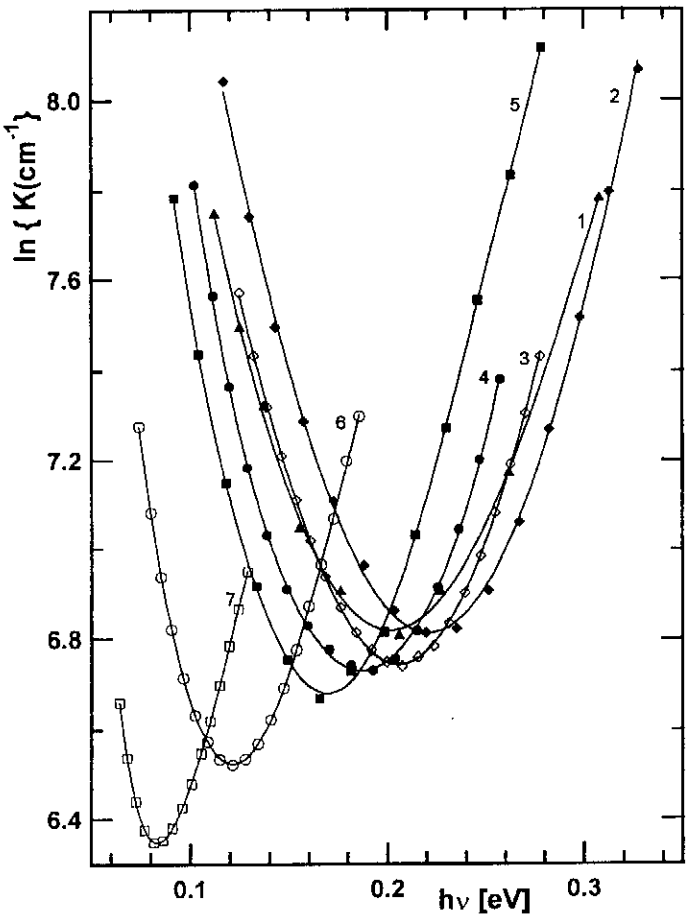

Fig. 6 Spectral dependences of the absorption coefficient K of $(Bi_{1-x}Sb_x)_2Se_3$ crystals (the samples are labelled according to Table II)

Tab. II Optical parameters of $(Bi_{1-x}Sb_x)_2Se_3$ single crystals

No.	x	ν_{min} cm^{-1}	ω_p $10^{13}s^{-1}$	τ 10^{-14} s	$M/m_\perp$ 10^{26} m^{-3}	ε_∞	K_{min} cm^{-1}	γ
1	0	760	13.6	6	1.74	29.8	902	2.3
2	0.012	795	14.1	5.34	1.86	29.7	907	2.4
3	0.04	708	12.5	5.3	1.48	29.8	846	2.3
4	0.082	633	11.2	5.71	1.15	29	837	2.5
5	0.098	587	10.3	6.05	0.95	28.3	788	2.5
6	0.136	513	9.1	6.43	0.73	27.5	679	2.4
7	0.163	463	7.8	6	0.5	26.3	567	2.2

where d is the sample thickness, to determine the absorption coefficient K as a function of the incident photon energy. The results are shown in Fig. 6.

The changes in the concentration of the free charge carriers, following from the analysis of the reflectance spectra, should manifest themselves by changes in the absolute value of the absorption coefficient K. One can expect an increase (possibly very slight only) in the value of K in the sample with the lowest value of x (sample No. 2), and, on the contrary, a decrease in K in the range of higher antimony content. Good agreement of the experiment with this assumption is evident in Fig. 6 and also from the values of the absorption coefficient K_{min} in the minima of the $K = f(h\nu)$ curves, presented in Table II. This finding allows us to assert that the results of the independent measurements of the reflectance and transmittance are in good agreement.

Further, a pronounced change in the location of the short-wavelength absorption edge is evident from the $K = f(h\nu)$ curves. The absorption edge of undoped Bi_2Se_3 is located near 0.20 eV. The short-wavelength absorption edge of the sample with the lowest Sb content (sample No. 2), as compared to that of Bi_2Se_3, is shifted towards higher photon energies. The location of the absorption edge of the sample No. 3 is virtually identical with that of undoped Bi_2Se_3. In other samples a shift of the absorption edge towards lower photon energies with growing Sb content is observed. This means that the substitution of Sb atoms for Bi in the Bi_2Se_3 crystal lattice results in an observable increase of the optical gap E_g^{opt} whereas the values of E_g^{opt} decrease with x in the $(Bi_{1-x}Sb_x)_2Se_3$ samples of higher Sb content. This fact can be qualitatively explained in the following way.

The location of the short-wavelength absorption edge, or its change, is a result of two factors:

a) variation of the gap width with composition in mixed semiconducting crystals of different gap widths ($E_g^{opt}(Bi_2Se_3)$ = 0.115 eV [20], ($E_g^{opt}(Sbi_2Se_3)$ = 1.2 eV

[21]—i.e. variation of the ionicity of the crystals: substitution of Sb atoms for Bi in the Bi_2Se_3 crystal leads to an increase in the gap width.

b) Moss-Burstein effect, i.e. the shift of the absorption edge resulting from the changes of the free carrier concentration N: an increase in N gives rise to a shift of the edge towards higher energies and, conversely, a decrease in the value of N shifts the edge towards higher energies.

Simultaneous action of both these factors can give rise to the experimentally observed variations of the optical gap width. In the sample with the lowest Sb con-

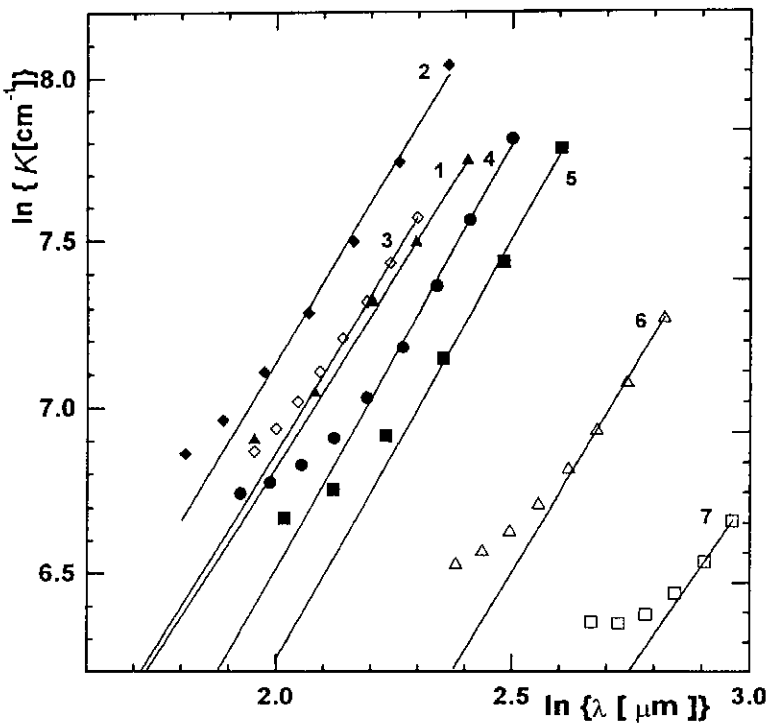

Fig. 7 Plots of $\ln K$ vs. $\ln\lambda$ For $(Bi_{1-x}Sb_x)_2Se_3$ crystals (the samples are labelled according to Table II)

tent the free carrier concentration increases, the increase in E_g^{opt} being given by the sum of both factors, whereas in the samples with higher Sb content (samples Nos 3–7) both factors counteract—the increase in the ionicity (sub a) shifts the absorption edge towards higher energies, on the other hand the Moss-Burstein effect (ad b) shifts the edge towards lower energies. The experiment shows that the action of the Moss-Burstein effect is dominant in the case of $(Bi_{1-x}Sb_x)_2Se_3$ crystals, the probable reason being in that the substitution of Sb atoms for Bi atoms in the crystal

Tab. III The values of the Hall constant $R_H(\boldsymbol{B}/\!/c)$, electric conductivity $\sigma\perp c$, Seebeck coefficient $\alpha(\Delta T\perp c)$, and product $R_H(\boldsymbol{B}/\!/c).\sigma\perp c$ of $(Bi_{1-x}Sb_x)_2Se_3$ crystals at temperature T = 300 K

No	x	$\alpha(\Delta T\perp c)$ $\mu V K^{-1}$	$\sigma_{\perp c}$ $10^3\ \Omega^{-1} m^{-1}$	$R_H(\boldsymbol{B}/\!/c)$ $10^{-6}\ m^3 A^{-1} s^{-1}$	$R_H.\sigma$ $10^{-3}\ m^2 V^{-1} s^{-1}$
1	0	-57	251	-0.22	55
2	0.012	-52	263	-0.19	50
3	0.076	-56	207	-0.32	66
4	0.098	-72	188	-0.45	85
5	0.163	-83	140	-0.73	102
6	0.203	-93	115	-1.01	116

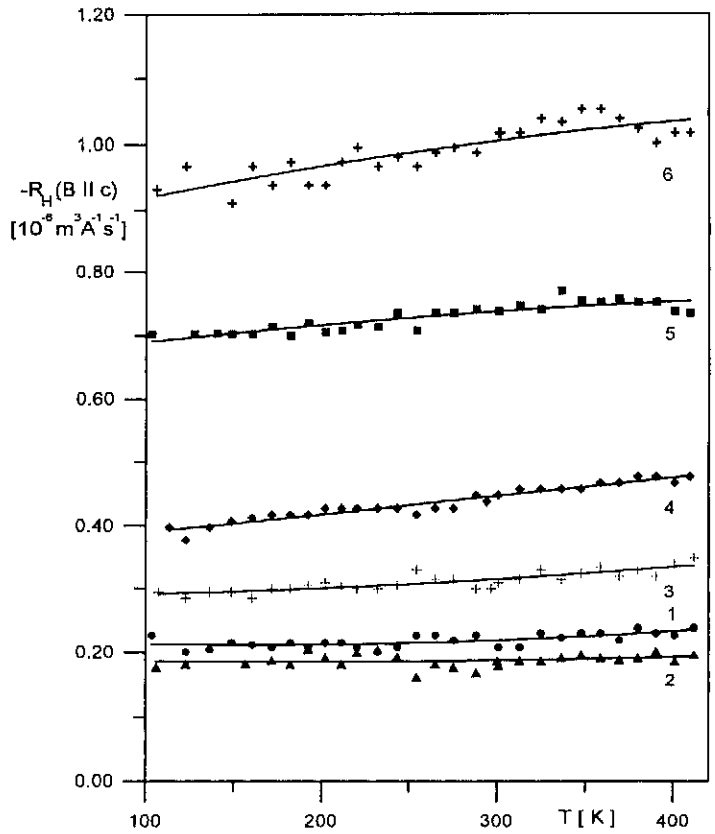

Fig. 8 Temperature dependences of the Hall constant $R_H(\boldsymbol{B}/\!/c)$ in $(Bi_{1-x}Sb_x)_2Se_3$ samples. The samples are labelled according to Table III

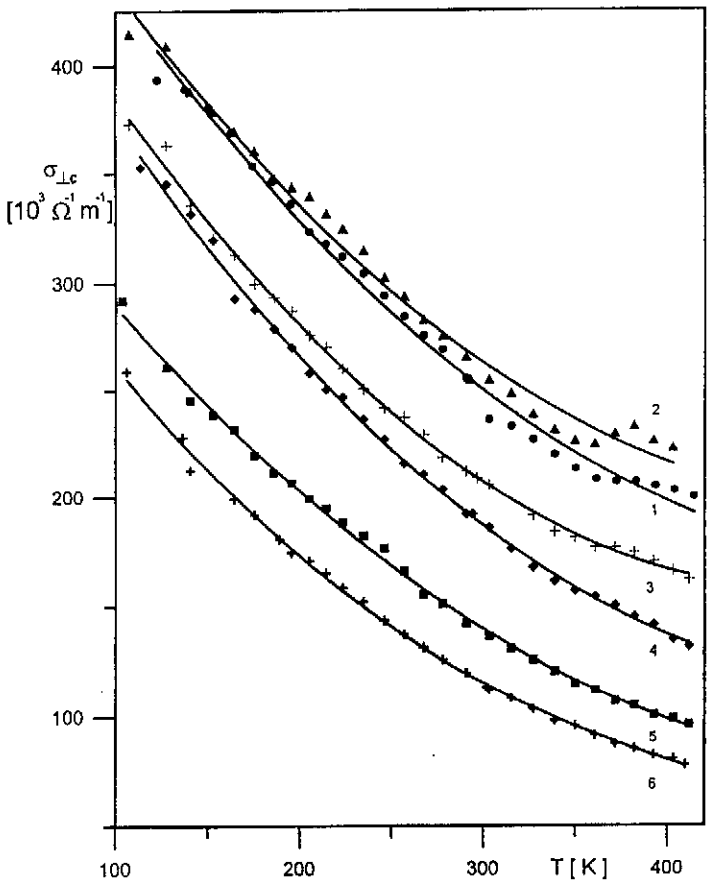

Fig. 9 Temperature dependences of the electrical conductivity $\sigma_{\perp c}$ in $(Bi_{1-x}Sb_x)_2Se_3$ samples. The samples are labelled according to Table III

lattice of Bi_2Se_3 results in a relatively pronounced decrease of the free charge carrier concentration. A more detailed analysis of this phenomenon has not been carried out in view of the fact that the action of both the effects mentioned cannot be separated on the basis of the given experimental data.

It is known that the shape of the long-wavelength edge gives information on the scattering mechanism of the free charge carriers. With the objective to determine the values of the exponent β in the relation $K \sim \lambda^{\beta}$, we have plotted the curves $\ln K$ vs. $\ln\lambda$ in Fig. 7. The values of β lie in the interval of $2.0 - 2.5$. This signifies that in $(Bi_{1-x}Sb_x)_2Se_3$ crystals ($x = 0.0 - 0.2$) at temperatures close to 300 K the dominant scattering mechanism of the free carriers is the scattering by the acoustic branches of lattice vibrations. The fact that the β values obtained are higher than 3/2, which according to paper [22] in covalent crystals correspond to the scattering

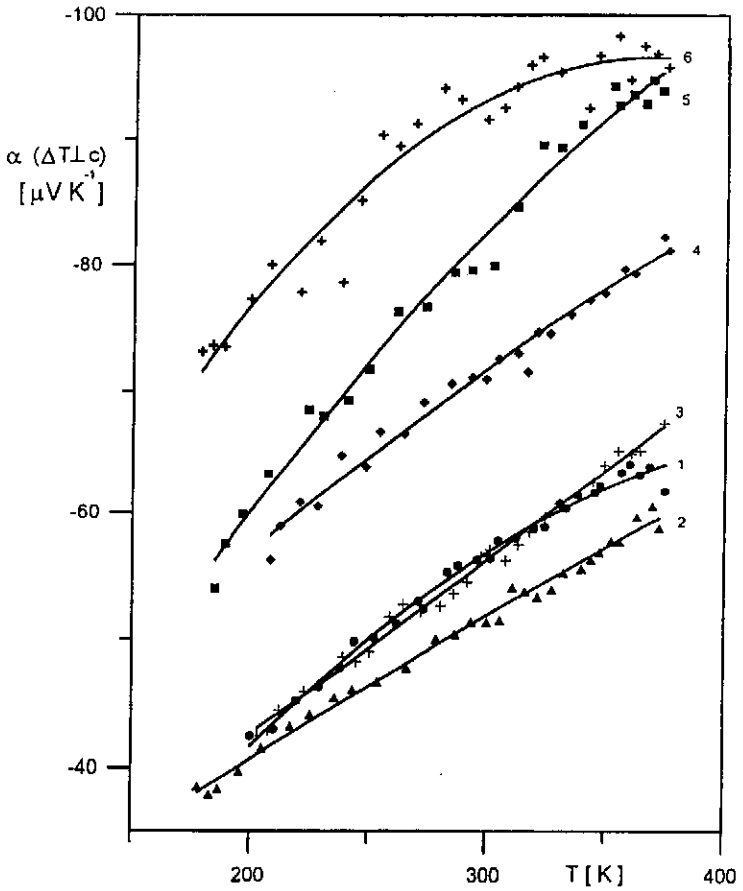

Fig. 10 Temperature dependences of the Seebeck coefficient $\alpha(\Delta T \perp c)$ in $(Bi_{1-x}Sb_x)_2Se_3$ samples; the samples are labelled according to Table III

by acoustic phonons, can be explained by assuming that in our mixed crystals we deal with a mixed scattering mechanism by acoustic phonons and by ionized impurities. This view is in full agreement with the conclusion of the paper by Stordeur et al. [4], implying that at room temperature the crystal lattice of Bi_2Se_3 is characterized by a mixed anisotropic scattering mechanism of the free carriers by acoustic phonons and ionized impurities.

Hall Constant, Electrical Conductivity and Seebeck Coefficient

$(Bi_{1-x}Sb_x)_2Se_3$ single crystals were characterized by the values of the Hall constant, electrical conductivity and Seebeck coefficient at room temperature in paper [8]. The

temperature dependences of the above-mentioned quantities along with the experimental techniques were described in paper [23].

The results of the measurements of the Hall constant $R_H(\boldsymbol{B}//c)$, electrical conductivity $\sigma_{\perp c}$ and Seebeck coefficient $\alpha(\Delta T \perp c)$ of the $(Bi_{1-x}Sb_x)_2Se_3$ crystal samples are summarized in Table III and shown in Figs 8 to 10. The presented results show an extrem for small concentration of antimony. With the aim to examine dependences of $R_H(\boldsymbol{B}//c) = f(x)$, $\alpha(\Delta T \perp c) = f(x)$ and $\sigma_{\perp c} = f(x)$ with regard to the above-mentioned extremes, the values of $R_H(\boldsymbol{B}//c)$, $\sigma_{\perp c}$ and $\alpha(\Delta T \perp c)$ were determined for a large set of samples with different x at $T = 300$ K (see Fig. 11). It is evident, that $R_H(\boldsymbol{B}//c)$ and $\alpha(\Delta T \perp c)$ in the region of small values of x de-

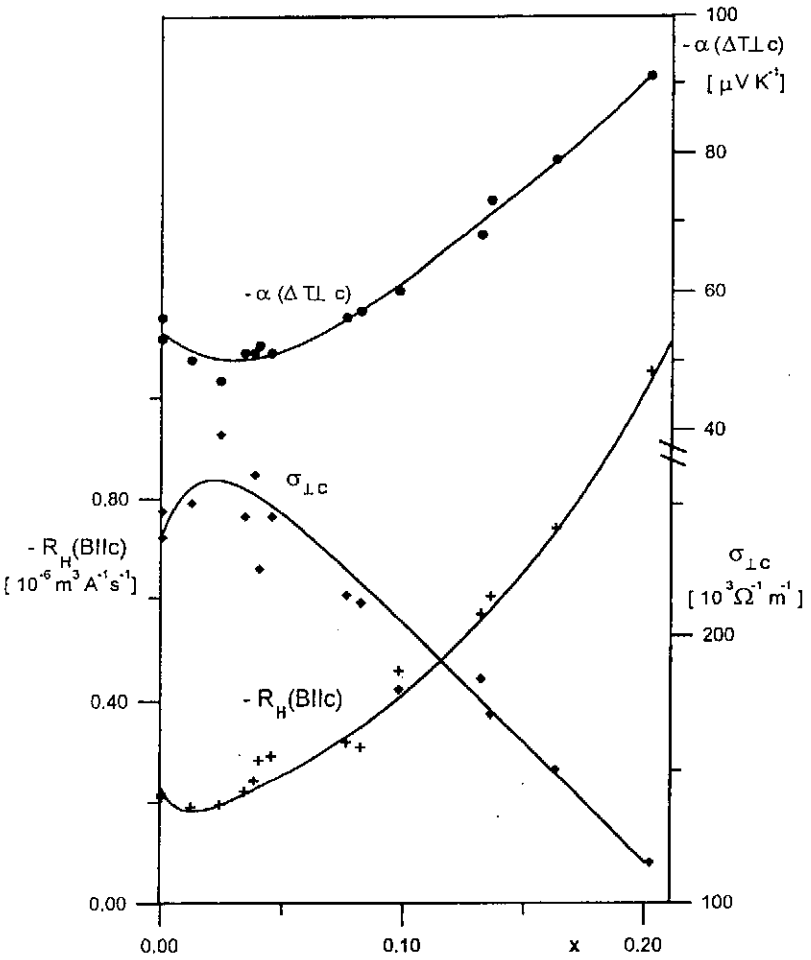

Fig. 11 Plots of the Hall constant $R_H(\boldsymbol{B}//c)$, electrical conductivity $\sigma_{\perp c}$ and Seebeck coefficient $\alpha(\Delta T \perp c)$ of $(Bi_{1-x}Sb_x)_2Se_3$ crystals against antimony content

crease and then, at higher values of x their magnitude increases. The electrical conductivity reaches a maximum in the region of small Sb contents, while at higher Sb contents the values of $\sigma \perp c$ decrease.

From the obtained results we conclude that the substitution of Bi atoms in Bi_2Se_3 by Sb atoms in the region of low Sb concentrations results in a concentration increase of free current carriers (free electrons), while at higher Sb concentrations the free carrier concentration decreases. This conclusion is in good agreement with the results obtained from measurements of reflectance in the plasma resonance region and with the measurements of transmittance in IR region [18].

It should be mentioned that a similar effect has been reported in paper [13]

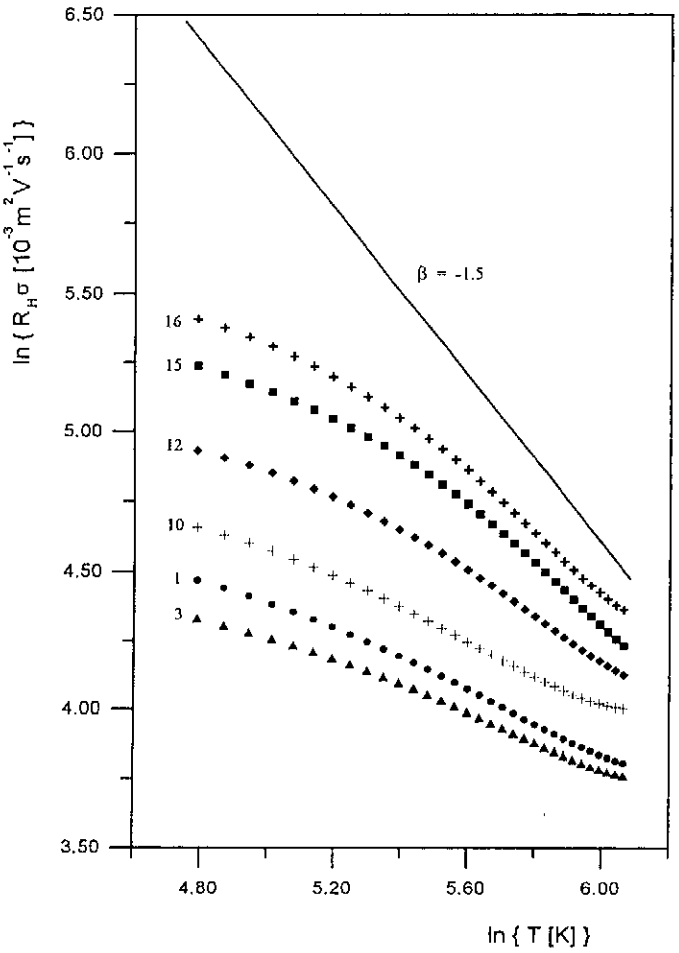

Fig. 12 Dependences of $\ln(R_H\sigma)$ on $\ln T$ in $(Bi_{1-x}Sb_x)_2Se_3$ samples; the samples are labelled according to Table III

on $(Bi_{1-x}In_x)_2Se_3$ crystals, where on substituting indium atoms for Bi atoms in the Bi_2Se_3 lattice we also observed an increase in the concentration of free electrons for a low indium content and its decrease at a higher indium content.

To evaluate the effect of the incorporation of Sb atoms into the Bi_2Se_3 crystal lattice on the mobility of free current carriers, the values of the product $R_H\sigma$ were calculated (see the last column of Table III). It is evident that a small Sb content in the samples leads to a decrease of in $R_H\sigma$ product, while at higher Sb content a significant increase in the value of $R_H\sigma$ product can be observed. From these data we concluded that the substitution of Bi atoms in the Bi_2Se_3 crystal lattice by Sb atoms results, in the region of small Sb concentrations, in a mobility decrease of free electrons, whereas at higher Sb concentrations the mobility of electrons significantly increases.

From the temperature dependence of the free carrier mobility it is possible to evaluate the character of the scattering mechanism. Therefore, in order to determine the value of γ in the expression of $\mu \approx R_H\sigma \approx T^\gamma$, the dependences of $\ln(R_H\sigma)$ vs. $\ln T$ are plotted in Fig. 12. In this Figure the line with a slope of $\gamma = -1.5$ represents a theoretical temperature dependence of the mobility of free current carriers for the case of the scattering of electrons on acoustical phonons.

The dependences of $\ln(R_H\sigma) = f(\ln T)$ obtained within the studied temperature region from 100 to 400 K have a substantially lower slope than $\gamma = -1.5$. This result leads to a conclusion that in the given temperature region the transport properties of the studied crystals of $(Bi_{1-x}Sb_x)_2Se_3$ can be characterized by a mixed scattering mechanism on the acoustical phonons and ionized impurities. This conclusion is in good agreement with the results presented in the paper by Stordeur et al. [4] for Bi_2Se_3.

Point Defects in $(Bi_{1-x}Sb_x)_2Se_3$ Crystals

In this section we shall make an attempt to account qualitatively for the variation of the concentration of free charge carriers in $(Bi_{1-x}Sb_x)_2Se_3$ crystals with x, following from the results of the reported measurements of the reflectance, transmittance, Hall constant, electrical conductivity and Seebeck coefficient.

Our considerations are based on the idea that the concentration of free charge carriers in the Bi_2Se_3 or $(Bi_{1-x}Sb_x)_2Se_3$ crystal lattice is determined by the character and concentration of lattice point defects. It is evident that mere substitution of antimony atoms for Bi in the Bi_2Se_3 crystal lattice, giving rise to uncharged substitution defects $Sb_{Bi}^{\times}$ of antimony atoms in bismuth sites, cannot account for the experimentally observed variations of the free electron concentration with x in $(Bi_{1-x}Sb_x)_2Se_3$ crystals. But when we consider a possibility of an interaction of $Sb_{Bi}^{\times}$ defects with the native lattice defects of the Bi_2Se_3 crystal lattice, we can explain the experimental results qualitatively in the following way:

The undoped Bi_2Se_3 crystals prepared from the melt of a stoichiometric composition always show a superstoichiometric bismuth content [14]. For this reason, the $Bi_{2+\delta}Se_3$ crystals always reveal *n*-type electrical conductivity, which is explained as being due to the presence of positively charged vacancies in the selenium sublattice—$V_{Se}^{\bullet\bullet}$. The excess of bismuth in these crystals results most probably also in the formation of antisite defects (AS defects) in the $Bi_{2+\delta}Se_3$ lattice formed by bismuth atoms replacing selenium atoms in their lattice sites and having one negative charge—$Bi_{Se}^{/}$. The concentration of free current carriers $[e^{/}]$ is thus given by the expression

$$[e^{/}] = 2[V_{Se}^{\bullet\bullet}] - [Bi_{Se}^{/}] \qquad (6)$$

where $[V_{Se}^{\bullet\bullet}]$ is the concentration of vacancies in the Se-sublattice and $[Bi_{Se}^{/}]$ is the concentration of AS defects.

Under these assumptions, we can explain the observed increase in the free electron concentration in the range of low Sb content as a consequence of the built-in antimony atoms, i.e. defects of the $Sb_{Bi}^{\times}$ type, which suppress the concentration of AS defects; it is clear from equation (6) that in this case the concentration of free electrons $[e^{/}]$ increases. The decrease in the electron concentration in the region with a higher Sb content is probably associated with the decrease in the concentration of $V_{Se}^{\bullet\bullet}$ vacancies. Therefore we suppose that the observed changes of the concentration of the free charge carriers with increasing x in $(Bi_{1-x}Sb_x)_2Se_3$ samples can be explained by supposing that the substitution of antimony atoms for Bi atoms results both in the elimination of AS defects and in the suppression of the concentration of $V_{Se}^{\bullet\bullet}$ vacancies. Equivalent formulation of this idea is that the substitution of Bi atoms by Sb atoms results in a decrease in the original non-stoichiometry of the Bi_2Se_3 bismuth selenide crystal lattice, i.e. in a decrease in the superstoichiometric content of Bi in the cation sublattice.

The model of point defects in these crystals, mentioned above, is supported by the arguments by van Vechten [24], who showed that in isostructure binary crystals it is possible to determine in which sublattice there is a higher or lower concentration of vacancies, according to the size of the vacancy surface area: the higher the surface area of a vacancy, the higher the energy required for its formation. Hence, in a given sublattice, there is a lower concentration of vacancies with a larger surface area and a higher concentration of vacancies with a lower surface area. These ideas have been verified on the properties of binary crystals of sphalerite and wurtzite structure.

Applying these ideas to ternary crystals with tetradymite structure, one can expect that on substitution of antimony atoms for the bismuth atoms in the cation sublattice of Bi_2Se_3 the "effective" radius of the atoms in the cation sublattice of $(Bi_{1-x}Sb_x)_2Se_3$ will decrease and that the concentration of vacancies in the cation

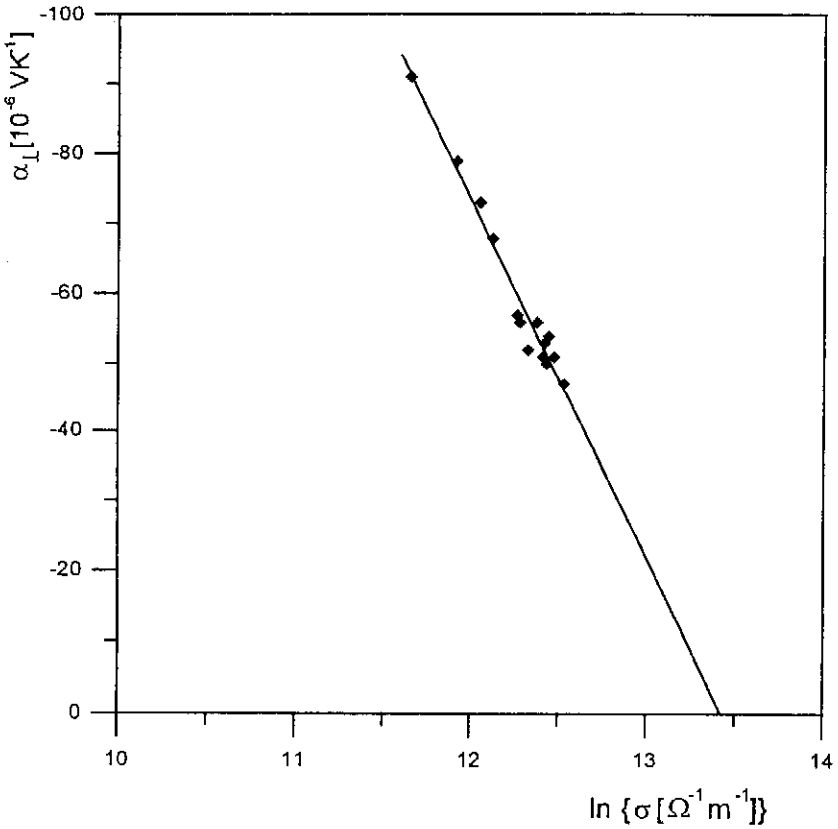

Fig. 13 $\alpha - \ln\sigma$ plot for $(Bi_{1-x}Sb_x)_2Se_3$ samples

sublattice will increase. Thus the substitution of antimony for Bi atoms results in the formation of vacancies in the cation sublattice. We can assume that these vacancies will be occupied by Bi atoms moving there from AS defects in the anion sublattice; the decrease of the concentration of AS defects will manifest itself by an increase of the free electron concentration. In the range of higher antimony content the dominant process is then the formation of vacancies in the cation sublattice. Taking into account that selenium vacancies $V_{Se}^{\bullet\bullet}$ remain in the crystal lattice, a further increase in the concentration of vacancies in the cation sublattice can be understood as a process which offsets the original non-stoichiometry of the crystal lattice (excess of Bi atoms); the decrease in non-stoichiometry will then manifest itself by a decrease in the concentration of free electrons, which is in agreement with experiment.

Power Factor and Figure of Merit

As mentioned in the introduction the figure of merit $Z = \sigma\alpha^2/\kappa$ is employed as a criterion for applicability of materials in thermoelectric devices. Because its experimental determination is tedious, a simpler metod for a fast evaluation of thermoelectric properties was suggested in paper [25].

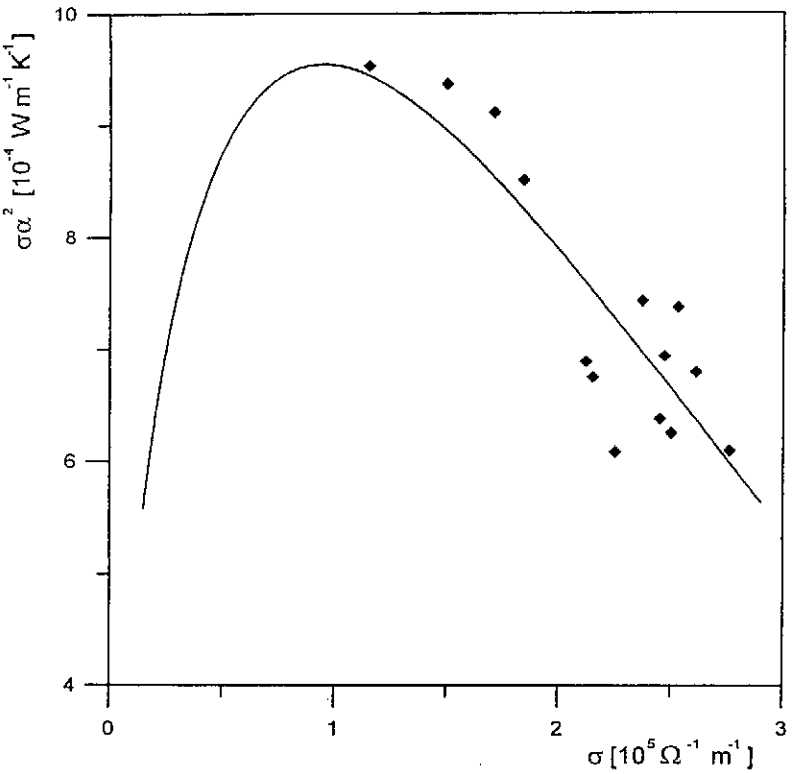

Fig. 14 The electrical power factor $\sigma\alpha^2$ as a function of the electrical conductivity σ for $(Bi_{1-x}Sb_x)_2Se_3$ crystals at T = 300 K

This method is based on the determination of optimal electrical conductivity σ_{opt} and the maximum electrical power factor $\sigma\alpha^2_{max}$. These quantities are determined by the equation expressing dependence of the Seebeck coefficient α on electrical conductivity σ as $\alpha = m(b - \ln\sigma)$. Plot of α vs. $\ln\sigma$ gives parameters m and b and thus enables the determination of σ_{opt} and $\sigma\alpha^2_{max}$. The optimum electrical conductivity σ_{opt} and the maximum electrical power factor $\sigma\alpha^2_{max}$ are given by the expression of $\sigma_{opt} = \exp(b - 2)$ and $\sigma\alpha^2_{max} = 4m^2\exp(b - 2)$, respectively. This method was verified in paper [25] on several types of materials using previously

published data.

The evaluation of $(Bi_{1-x}Sb_x)_2Se_3$ samples using the above-mentioned method is presented in paper [26]. The dependence $\alpha = f(\ln\sigma)$ is demonstrated in Fig. 13. It is evident that the experimental data obey the linear function $\alpha = m(b - \ln\sigma)$. That is why the method seems to be applicable to the first evaluation of thermoelectric properties of $(Bi_{1-x}Sb_x)_2Se_3$ samples despite the rough simplification mentioned in paper [25].

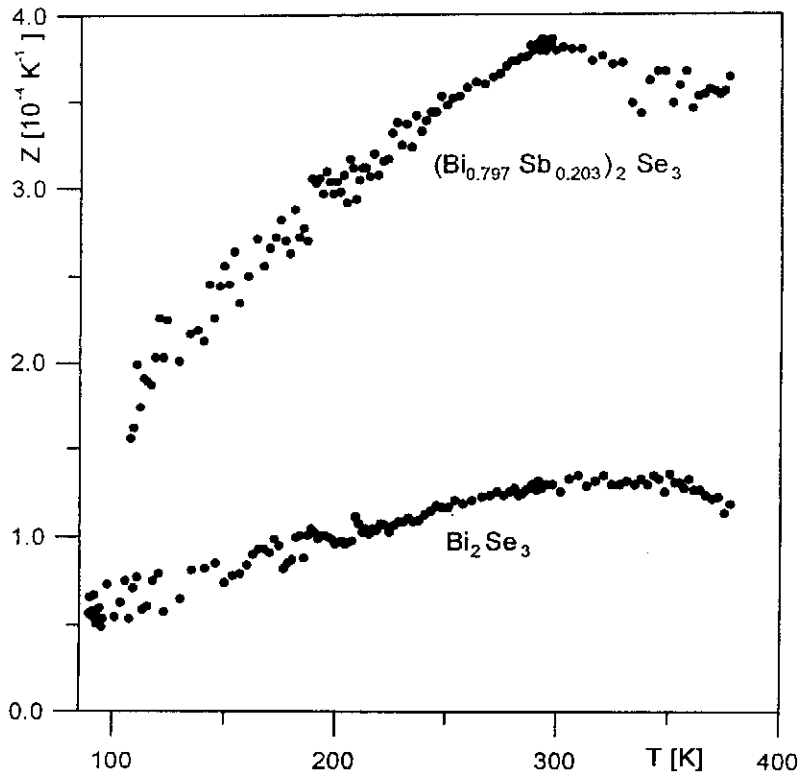

Fig. 15 Temperature dependences of the figure of merit Z for Bi_2Se_3 and $(Bi_{0.797}Sb_{0.203})_2Se_3$

From the plot in Fig. 13 the parameters b and m were determined: $b = 13.4\ \ \Omega^{-1}\,m^{-1}$ and $m = 50\ \ \mu V\,K^{-1}$. Using these data the values of $\sigma_{opt} \approx 9\times10^4\ \ \Omega^{-1}\,m^{-1}$, $\sigma\alpha^2_{max} \approx 9.4\times10^{-4}\ \ W\,m^{-1}\,K^{-2}$ and the course of the function $\sigma\alpha^2 = f(\sigma)$ were calculated. The function $\sigma\alpha^2 = f(\sigma)$ is shown in Fig. 14. The experimental data are represented by dots. It can be seen that the experimental data are in good agreement with the calculated curve.

It can be seen that the values of $\sigma\alpha^2$ corresponding to the sample with the highest content of Sb ($x = 0.203$) are located in the region of maximum of the

curve. Similarly, the value of electrical conductivity of the sample ($\sigma = 1.15\times10^5$ $\Omega^{-1}\,m^{-1}$) is closed to the optimum electrical conductivity ($\sigma_{opt} \approx 9\times10^4\ \Omega^{-1}\,m^{-1}$). Samples with higher concentration of Sb and thus lower electrical conductivity were not prepared due to the formation of another phase [5].

From Fig. 14 it is evident that the electrical power factor increases on substituting Bi atoms for Sb atoms in Bi_2Se_3 crystal lattice. One can conclude that the formation of solid solutions improves thermoelectric properties of starting Bi_2Se_3 as regards applications. This conclusion is supported by the measurements of figure-of-merit [26] resulting from Harman's technique [27]. In Fig. 15 the measurements of Z are illustrated for boundary composition ($x = 0$ and $x = 0.203$). It can be seen that the figure of merit of $(Bi_{0.797}Sb_{0.203})_2Se_3$ sample is about four times higher than that of Bi_2Se_3. Despite this improvement, the values of z of the materials prepared are by one order smaller than those of the materials used for industrial applications. Although the figure of merit would be probably higher if the lattice thermal conductivity and electron concentration were optimized separately, the results presented indicate that this system will not probably be usable for thermoelectric applications.

Conclusion

The single crystals of $(Bi_{1-x}Sb_x)_2Se_3$ solid solutions ($x = 0.00 - 0.20$), prepared by a modified Bridgman method were characterized by means of the X-ray diffraction analysis, homogeneity assessment, and measurements of the reflectance in the plasma resonance range, transmittance, electrical conductivity $\sigma\perp c$, Hall constant $R_H(\boldsymbol{B}\|c)$, Seebeck coefficient $\alpha(\Delta T\perp c)$ and figure of merit Z.

It was found that the substitution of Bi atoms by Sb atoms in the Bi_2Se_3 crystal lattice in the region of small Sb concentrations leads to an increase in the concentration of free electrons N, whereas in the region of higher Sb concentrations the values of N decrease.

The observed effect can be explained qualitatively assuming that the incorporation of Sb atoms into the Bi_2Se_3 lattice results in a suppression of native defects of this lattice, i.e. in a decrease in the concentration of vacancies in the anion sublattice $V_{Se}^{\bullet\bullet}$ and antisite defects $Bi_{Se}^{/}$.

From the analysis of the dependences of $\ln(R_H\sigma) = f(\ln T)$ we have concluded that in the temperature range of 100 – 400 K the transport properties of the $(Bi_{1-x}Sb_x)_2Se_3$ crystals can be described by a mixed scattering mechanism of free current carriers on acoustical phonons and ionized impurities. This conclusion is strengthened by the analysis of long wavelength edge (it was found that the values of the exponent β in the relation $K \sim \lambda^{\beta}$ lie in the interval from 2.2 to 2.5.

Substitution of Sb for Bi atoms in Bi_2Se_3 (that means formation of solid solution $(Bi_{0.797}Sb_{0.203})_2Se_3$ leads to an increase in the figure-of-merit. Despite this

improvement, the values of Z of the best of the materials prepared are by one order smaller than those of the materials used for construction of solid state coolers and thermoelectric generators. Thus these solid solutions are not useful in thermoelectric applications.

References

1. Stordeur M: *CRC Handbuch of Thermoelectrics*, (D.M. Rowe, ed.), p. 240, CRC Press, Boka Radon, New York 1995.
2. Krost A: Landolt-Börnstein, New Series Group III, Vol.17, Subvol. f, p. 268, Springer, Berlin 1983.
3. .Horák J., Starý Z., Lošťák P., Pancíř J.: J. Phys. Chem. Solids **51**, 1353 (1990).
4. .Stordeur M., Ketavong K. K., Priemuth A., Sobotta H., Riede V.: Phys. Status Solidi **169**, 505 (1992).
5. .Kuznetsov V. G., Palkina K. K., Reshchikova A. A.: Izv. Akad. Nauk SSSR, Neorg. Mater. **4**, 670 (1968).
6. Dmitriev A. V., Kuznetsov V. G., Reshchikova A. A.: Izv. Akad. Nauk SSSR, Neorg. Mater. **4**, 1917 (1968).
7. Tichý L., Vít V., Florián Č., Frumar M.: Phys. Status Solidi (a) **58**, K43 (1980).
8. Lošťák P., Drašar Č., Süssman H., Reinshaus P., Novotný R., Beneš L.: J. Cryst. Growth **179**, 144 (1997).
9. Gobrecht H., Boerets K. E., Pantzer G.: Z. Physik **177**, 68 (1964).
10. Abrikosov N.Kh., Bankina V.F., Khazimonovich K.F.: Zh. Neorg. Khim. **5**, 2021 (1960).
11. Wobst M.: Scripta Metalurg. **5**, 583 (1971).
12. Süssman H., Bohm M., Reinshaus P.: *Proc. 12th. Inter. Conf. on Thermoelectrics*, p. 86, Yokohama 1993.
13. Lošťák P., Beneš L., Civiš S., Süssman H.: J. Mater. Sci. **25**, 277 (1990).
14. Offergeld G., van Cakenberghe J.: J. Phys. Chem. Solids **11**, 310 (1959).
15. Bogatyrev I.F., Vaško A., Tichý L., Horák J.: Phys. Status Solidi (a) **22**, K63 (1973).
16. Horák J., Karamazov S., Lošťák P.: Radiation Effects and Defects in Solids **140**, 181 (1997).
17. Gobrecht H., Seek S., Klose T.: Z. Physik **190**, 427 (1966).
18. Navrátil J., Lošťák P., Drašar Č., Blachut T.: Phys. Status Solidi (b) **194**, 783 (1996).
19. Madelung O.: *Handbuch der Physik*, (S. Flügge, ed.), Vol. 20, p. 210, Springer, Berlin 1957.
20. Köhler H., Hartmann J.: Phys. Status Solidi (b) **63**, 171 (1974).
21. Black J., Conwell E.M., Seigle L., Spencer C.W.: J. Phys. Chem. Solids **2**, 240

(1957).
22. Lisica M.P., Malinko V.N., Podlinskii J.V., Cebulya G.G.: Ukr. Fiz. Zh. **8**, 1298 (1969).
23. Drašar Č., Klichová I., Koudelka L., Lošťák P.: Cryst. Res. Technol. **31**, 805 (1996).
24. van Vechten A.: J. Electrochem. Soc. **122**, 419 (1975).
25. Rowe D.M., Gao Min, Williams S.G.K.: *Proc. 14th Inter. Conf. on Thermoelectrics*, p. 288, St. Peterburg 1995.
26. Drašar Č., Lošťák P., Navrátil J.: Materials Letters, submitted.
27. Starý Z., Navrátil J., Plecháček T.: *Proc. 13th Inter. Conf. on Thermoelectrics*, p. 286, Kansas City 1994.